

Effects of layer stacking and strain on electronic transport in two-dimensional tin monoxide

Yanfeng Ge(盖彦峰), Yong Liu(刘永)

Citation: Chin. Phys. B . 2019, 28(7): 077104. **doi:** 10.1088/1674-1056/28/7/077104
Journal homepage: http://cpb.iphy.ac.cn; http://iopscience.iop.org/cpb

What follows is a list of articles you may be interested in

Room-temperature infrared photodetectors with hybrid structure based on two-dimensional materials

Tiande Liu(刘天德), Lei Tong(童磊), Xinyu Huang(黄鑫宇), Lei Ye(叶镭)

Chin. Phys. B . 2019, 28(1): 017302. **doi:** 10.1088/1674-1056/28/1/017302

The superconducting properties of a Pb/$MoTe_2$/Pb heterostructure:First-principles calculations within the anisotropic Migdal-Eliashberg theory

Wei Xia(夏威), Jie Zhang(张洁), Gui-Qin Huang(黄桂芹)

Chin. Phys. B . 2018, 27(12): 126302. **doi:** 10.1088/1674-1056/27/12/126302

Effect of aperture field distribution on the maximum radiated power at atmospheric pressure

Pengcheng Zhao(赵朋程), Lixin Guo(郭立新)

Chin. Phys. B . 2017, 26(11): 115101. **doi:** 10.1088/1674-1056/26/11/115101

A facile and efficient dry transfer technique for two-dimensional Van der Waals heterostructure

Li Xie(谢立), Luojun Du(杜罗军), Xiaobo Lu(卢晓波), Rong Yang(杨蓉), Dongxia Shi(时东霞), Guangyu Zhang(张广宇)

Chin. Phys. B . 2017, 26(8): 087306. **doi:** 10.1088/1674-1056/26/8/087306

Au and Ti induced charge redistributions on monolayer WS_2

Zhu Hui-Li, Yang Wei-Huang, Wu Ya-Ping, Lin Wei, Kang Jun-Yong, Zhou Chang-Jie

Chin. Phys. B . 2015, 24(7): 077301. **doi:** 10.1088/1674-1056/24/7/077301

Effects of layer stacking and strain on electronic transport in two-dimensional tin monoxide*

Yanfeng Ge(盖彦峰) and Yong Liu(刘永)†

State Key Laboratory of Metastable Materials Science and Technology and Key Laboratory for Microstructural Material Physics of Hebei Province, School of Science, Yanshan University, Qinhuangdao 066004, *China*

(Received 7 January 2019; revised manuscript received 2 May 2019; published online 11 June 2019)

Tin monoxide (SnO) is an interesting two-dimensional material because it is a rare oxide semiconductor with bipolar conductivity. However, the lower room temperature mobility limits the applications of SnO in the future. Thus, we systematically investigate the effects of different layer structures and strains on the electron–phonon coupling and phonon-limited mobility of SnO. The A_{2u} phonon mode in the high-frequency region is the main contributor to the coupling with electrons for different layer structures. Moreover, the orbital hybridization of Sn atoms existing only in the bilayer structure changes the conduction band edge and conspicuously decreases the electron–phonon coupling, and thus the electronic transport performance of the bilayer is superior to that of other layers. In addition, the compressive strain of $\varepsilon = -1.0\%$ in the monolayer structure results in a conduction band minimum (CBM) consisting of two valleys at the Γ point and along the M–Γ line, and also leads to the intervalley electronic scattering assisted by the $E_{g(-1)}$ mode. However, the electron–phonon coupling regionally transferring from high frequency A_{2u} to low frequency $E_{g(-1)}$ results in little change of mobility.

Keywords: two-dimensional materials, tin monoxide, electronic transport, electron–phonon coupling

PACS: 51.50.+v, 63.20.kd, 63.20.dk, 73.90.+f **DOI:** 10.1088/1674-1056/28/7/077104

1. Introduction

It is well known that dimension plays one of the crucial roles in the properties of materials because the dimensionality reduction can give rise to significant changes. Thus, since the discovery of graphene, we have witnessed an explosion of interest in developing two-dimensional (2D) materials and understanding their properties.[1,2] A common characteristic of 2D materials is the weak van der Waals interaction between the layers and strong bonding within the layers. Beyond the graphene, 2D materials, such as *X*enes,[3–5] metal chalcogenides,[6–8] *MX*enes,[9,10] layered oxide materials,[11,12] and others,[13–16] have received considerable attention. The most monumental reason for this is that many motivating properties only exist in 2D materials. For example, the suitable bandgap, ultrahigh carrier mobility, and other novel quantum effects make them suitable for use in electronic, optical, and logic devices.[17–20]

Among the 2D materials, IV–VI compounds provide an opportunity for sustainable electronic and photonic systems due to their various structures, abundance in the earth, and nontoxic characteristics.[8,21] The ultrathin IV–VI compounds (SnS,[22–25] SnSe,[26,27] and SnSSe[28]) have been mechanically exfoliated and applied in high-performance field effect transistors. In addition, IV–VI compounds have demonstrated many interesting physical properties that are worthy of in-depth study.[29] For example, the direct bandgap of ~ 1.5 eV makes SnS have a high absorption coefficient, and a promising candidate for solar cells, photodetectors, and photocatalytic water splitting.[30–32] The transformation from the amorphous to the crystalline state of SnSe under a laser showed its advantage over memory devices.[33–35] Theoretical work also predicted that SnSe has a layer-dependent bandgap and can transit from an indirect to a direct bandgap semiconductor when the thickness decreases to a monolayer, thus indicating its potential applications in optical and optoelectronic devices.[36] Furthermore, multiferroics,[37,38] piezoelectric,[39,40] and topological insulators[41–43] have also been predicted in the family of IV–VI compounds, greatly extending their future applications.

Tin monoxide (SnO) is an interesting semiconductor and shows promise for a wide variety of technological applications.[44] The stable phase of SnO has a tetragonal crystallographic structure (*P*4/*nmm* space group[45–47]). The specific lone pair[48] of 5s electrons in SnO leads to the dipole–dipole interaction and the unique structure versus other IV–VI compounds, which makes SnO a rare oxide semiconductor with bipolar conductivity.[49–51] The van der Waals interaction along the [001] crystal direction also makes SnO form a layered structure with the Sn–O–Sn sequence,[52–54] as shown in Fig. 1. Due to the large direct optical bandgap,[55–58] the possible coexistence of electrical conductivity and optical transparency makes it ideal for invisible electronic devices.[59] As an essential physical property of the application potential in

*Project supported by the National Natural Science Foundation of China (Grant No. 11747054), the Specialized Research Fund for the Doctoral Program of Higher Education of China (Grant No. 2018M631760), the Project of Hebei Educational Department, China (Grant Nos. ZD2018015 and QN2018012), and the Advanced Postdoctoral Programs of Hebei Province, China (Grant No. B2017003004).

†Corresponding author. E-mail: yongliu@ysu.edu.cn

© 2019 Chinese Physical Society and IOP Publishing Ltd

multifunctional electronic devices, the electronic transport of SnO has been reported by many experimental studies. Field effect transistors using SnO have been developed[19,60–63] and show P-type conduction with the room temperature mobility $\sim 1\ \mathrm{cm}^2/(\mathrm{V\cdot s})$, which is much lower than that of MoS_2[17,64,65] and phosphorene,[66] and also limits the use of SnO in the future. The improvement of the mobility by the executable experimental method becomes a problem that demands prompt solution.

In experiments, several kinds of preparation methods[67] can control the production of high-quality 2D materials with a selected number of layers. It is found that many physical properties, especially the band edge structure, depend strongly on the number of layers. The twist angle between adjacent layers[68–71] can also affect electron structure. Moreover, strain engineering[72] has been successfully used to tailor the properties of 2D materials,[73–76] such as the crystal structure, bandgap, phonon, and so on. In order to study the effects of the above experimental methods on the electronic transport in SnO and provide the necessary calculation basis for the multifunctional applications of SnO, here, we study the electron–phonon coupling and phonon-limited mobility[77,78] of SnO modulated by different layer structures and strains based on first-principles calculations with Boltzmann transport theory. It is found that the A_{2u} phonon mode in the high-frequency region contributes to the major electron–phonon coupling for different layer structures. It is noteworthy that the significant change in the conduction band edge of the bilayer results in a huge reduction of electron–phonon coupling, thus improving the electronic transport performance. In the monolayer structure, although the compressive strain of $\varepsilon = -1.0\%$ greatly impacts the conduction band edge and changes the region of the main electron–phonon coupling in the phonon spectrum, its comprehensive effect on the mobility is minimal when the other strains also have little effect on the electronic transport.

2. Methods

Our calculation is based on the semiclassical Boltzmann transport theory. The transport electron–phonon coupling constant λ_{tr} can be obtained by

$$\lambda_{\mathrm{tr}} = 2\int_0^{\infty} \omega^{-1}\alpha_{\mathrm{tr}}^2 F(\omega)\mathrm{d}\omega, \tag{1}$$

where $\alpha_{\mathrm{tr}}^2 F(\omega)$ is the transport spectral function.[79] The relaxation time τ and the temperature dependence of mobility $\mu(T)$ can be expressed as

$$\tau^{-1} = \left(\frac{4\pi k_{\mathrm{B}}T}{\hbar}\right)\int \frac{\mathrm{d}\omega}{\omega}\frac{\tilde{\omega}^2}{\sinh^2\tilde{\omega}}\alpha_{\mathrm{tr}}^2 F(\omega), \tag{2}$$

$$\mu(T) = \frac{2eN_F\langle v_x^2\rangle}{n_{2\mathrm{D}}S_{\mathrm{cell}}}\tau, \tag{3}$$

where $\langle v_x^2\rangle$ is the average square of the Fermi velocity along the x direction, and S_{cell} is the area of the unit cell. The above method of electronic transport includes the coupling of all phonon modes in the dense q grid with the electrons, and is more comprehensive than the deformation potential theory[78], which involves only the effect of the longitudinal acoustic phonon mode.

The technical details of the calculations are as follows. All calculations, including the electronic structures, the phonon spectra, and the electron–phonon couplings, were carried out using the ABINIT package[80–83] with the local-density approximation. The ion and electron interactions were treated with the Hartwigsen–Goedecker–Hutter pseudopotentials.[84] The strain was introduced by adjusting the lattice constant a of the monolayer SnO with the strain capacity $\varepsilon = (a - a_0)/a_0 \times 100\%$. By requiring a convergence of the results, the kinetic energy cutoff of 600 eV and the Monkhorst–Pack k-mesh of $30 \times 30 \times 1$ were used in all calculations about the electronic ground-state properties. The phonon spectra and the electron–phonon couplings were calculated on a $15 \times 15 \times 1$ q-grid using the density functional perturbation theory (DFPT).[85] Because of the semiconductive property of SnO, carrier doping was necessary for the study of electronic transport properties, and we only considered electron doping with a doping concentration $n_{2\mathrm{D}} = 0.5 \times 10^{13}\ \mathrm{cm}^{-2}$. It was a reasonable value for the experimental doping technology and made the Fermi level locate around the conduction band edge.

3. Results

3.1. Number of layers and stacking effects

The monolayer SnO consists of three atomic layers, with the oxygen layer sandwiched between two tin layers (Fig. 1(a)). The equilibrium lattice constant is found to be $a_0 = b_0 = 3.835$ Å. The corresponding band structure shows a direct bandgap of ~ 2.5 eV with both the valence band maximum (VBM) and conduction band minimum (CBM) located around the Γ point (Fig. 1(a)). The band structure near the VBM is an approximate local flat band that results in the heavy electronic effective mass.

Furthermore, the number of layers and stacking types are also considered in the present work. First, the prototypical bilayer structure (denoted by bilayer for simplicity) is similar to the bulk structure ($P4/nmm$) but has a vacuum layer of 16 Å in order to be a 2D structure (Fig. 1(b)). The space between two adjacent Sn in different layers is 2.67 Å along the z-axis and includes the midpoint of a and b lattice vectors. The band structure of the bilayer shows that the CBM changes from the Γ point (Sn: p_y orbit) to the M point (Sn: $s+p_z$ orbits),[48] and the valence band around the Γ point (Sn: p_y orbit) has a Mexican-hat-like band structure (Fig. 1(e)). The indirect bandgap of ~ 1.0 eV in the bilayer is much narrower

than that of the monolayer, which is obviously different from the other 2D materials.[68,69] The important cause is the interlayer Sn–Sn interactions,[48] despite the weak van der Waals interactions between adjacent layers. The corresponding weak orbital hybridization of Sn atoms in different layers leads to bonding–antibonding splitting, which is inversely proportional to the space between two Sn atoms. Second, one of the bilayers is translated one-half lattice constant along the *b*-axis to constitute the new bilayer structure (denoted by T-bilayer for simplicity), as shown in Fig. 1(c). The space between two adjacent Sn in different layers is 4.05 Å along the *z*-axis, which is larger than that in the bilayer, and results in smaller bonding–antibonding splitting. Thus, the band structure of the T-bilayer is similar to the monolayer with a smaller bandgap of ~ 1.9 eV (Fig. 1(f)). Moreover, the Mexican-hat-like band or flat band around the VBM in three structures gives rise to low P-type carrier mobility, and therefore only the N-type carrier is considered in the present work.

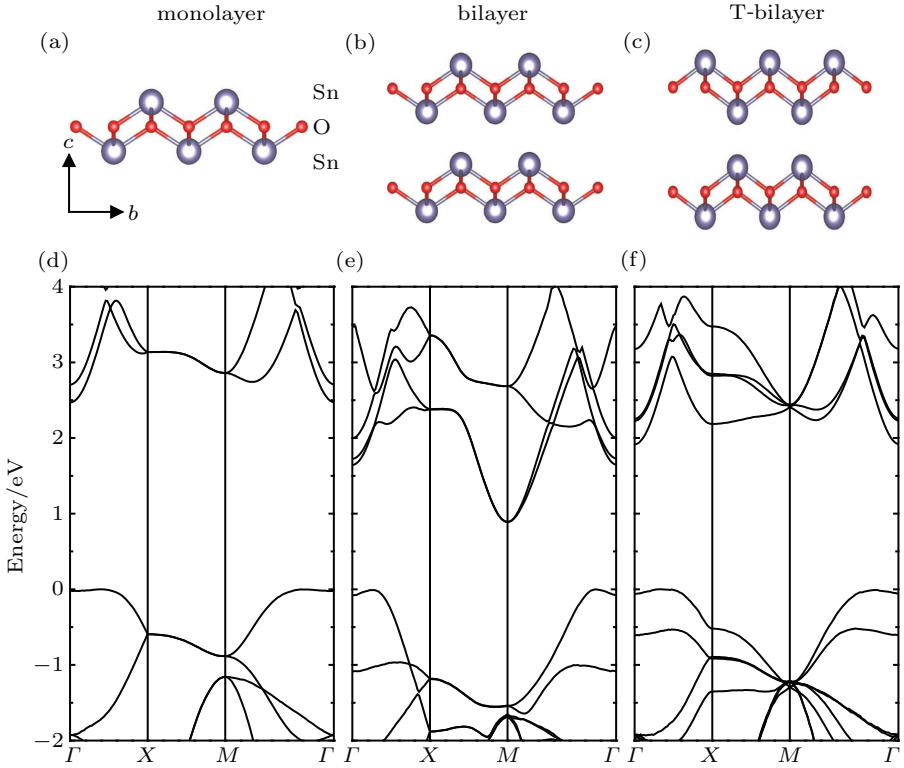


Fig. 1. Lattice structures of the (a) monolayer, (b) bilayer, and (c) T-bilayer, and the band structures of the (d) monolayer, (e) bilayer, and (f) T-bilayer. The monolayer structure has a direct bandgap of ~ 2.5 eV at the Γ point. Both types of bilayers have indirect bandgaps, which are ~ 1.0 eV and ~ 1.9 eV, respectively. The VBM and CBM of the T-bilayer structure are located around the Γ point. However, the CBM of the bilayer structure around the *M* point is distinctly different from that in the other two cases.

By using the DFPT, we calculated the phonon spectra and the electron–phonon couplings of the monolayer, bilayer, and T-bilayer. As shown in Fig. 2, the absence of imaginary frequency in the phonon spectra ensures the dynamic stabilities of the three cases. According to the group theory, the following five irreducible representations at the Γ point are used to denote the optic vibrational modes: $\Gamma = A_{1g} + B_{1g} + 2E_g + A_{2u} + E_u$.[19] Figure 2(d) shows the three main optical vibration modes (A_{2u}, $E_{g(-1)}$, and $E_{g(-2)}$) that are strongly coupling with electrons, as demonstrated in the following discussions. The magnitude of the phonon linewidth is indicated by the size of the red error bar in Fig. 2. It is found that the high-frequency phonon in the range of 350–400 cm^{-1} has the largest phonon linewidth in the monolayer SnO, corresponding to the relative vibration between the Sn sublattice and the O sublattice in the *xy* plane (irreducible representation: A_{2u}). With regard to the bilayer, due to the significant changes in the conduction band, the values of the phonon linewidth decrease markedly, as shown in Fig. 2(b). The phonon linewidth of the T-bilayer is slightly smaller than that of the monolayer for the analogical band structures.

As shown in Fig. 3(a), the main peaks in the transport spectral function α_{tr} of the monolayer also demonstrate that the strong electron–phonon coupling is derived from the phonon in the range of 350–400 cm^{-1}, in accordance with the above results of phonon linewidths; the same is true for the case of the T-bilayer. In contrast, the much smaller phonon linewidths of the bilayer generate the lower peak in the overall transport spectral function. According to Eq. (3), the electronic relaxation times τ of three cases are shown in Fig. 3(b). The monolayer and T-bilayer have close results due to their similar band structure, phonon spectra, and phonon linewidths. Both cases have τ of ~ 10 fs at room temperature. Moreover, the weaker electron–phonon coupling of the bilayer gives rise to a much longer electronic relax time than the monolayer and T-bilayer, such as when $\tau = 20$ fs at room temperature.

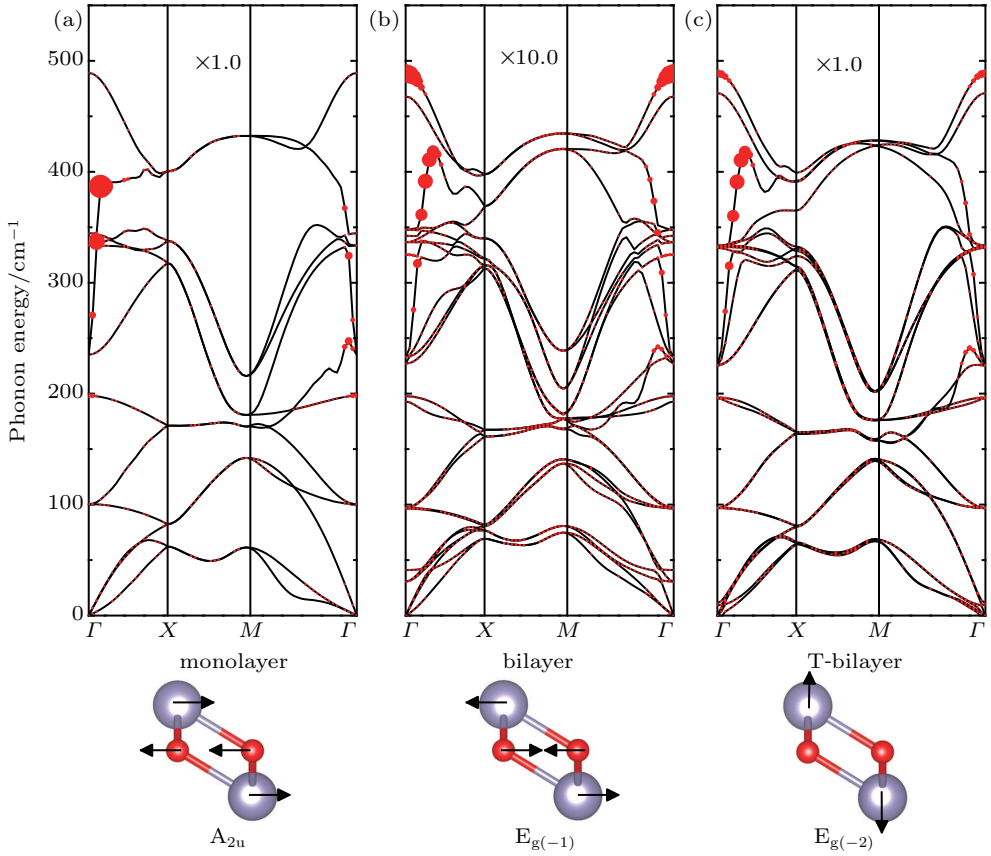


Fig. 2. Phonon spectra and phonon linewidths of the (d) monolayer, (e) bilayer, and (f) T-bilayer. The magnitude of the phonon linewidth is indicated by the size of the red error bar, and the magnitude for the bilayer is plotted with ten times the real values. The large phonon linewidths mainly focus on the Γ point in the high-frequency region (350 $\sim$ 400 cm^{-1}).

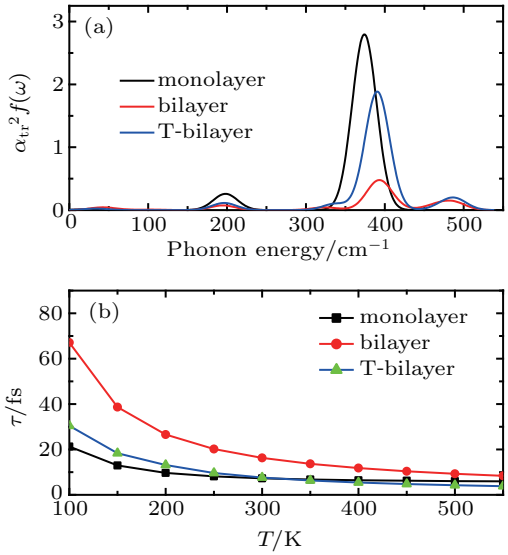


Fig. 3. (a) Transport spectral functions α_{tr} of the monolayer, bilayer, and T-bilayer. The main peak appears at $\sim$ 380 cm^{-1} in the high-frequency region, which is consistent with the results of phonon linewidths. The peak value of the bilayer is much lower than those of the other two cases. (b) The electronic relaxation time τ of the monolayer, bilayer, and T-bilayer as a function of temperature T.

3.2. Strain effect

In addition to the effects of the number of layers and stacking types, we also study the influences of different extents and types of strains in the monolayer structure, including tensile and compressive strains. To ensure the dynamic stability of lattice structures, only strains of no more than 1% are considered in the present work, which will be discussed later. Under compressive strains, the conduction bands around points X and M are gradually approaching the CBM with the increase in strain, as shown in Fig. 4. In particular, the compressive strain of $\varepsilon = -1.0\%$ makes the CBM consist of two parts: the valleys at the Γ point and the valleys along the M–Γ line. However, the tensile strains have little impact on the CBM except for the slight rise in conduction bands around the X point.

In the phonon spectra of different extents and types of strains (Fig. 5), it is found that compressive strains increase atomic vibration frequencies due to the reduction in the distance between atoms and the strengthening of the bond energy, which is just opposite to the tensile strains. Because two tensile strains and the compressive strain of $\varepsilon = -0.5\%$ have almost no influence on the conduction band edge, the results about phonon linewidths show similar little effect of strains. For the case of $\varepsilon = -1.0\%$, the region of large phonon linewidths occurs in the medium frequency and mainly contains two parts of compositions: at the Γ point and at the midpoint of the Γ–X line. Both phonon modes belong to the irreducible representations of E$_g$. One is the in-plane vibrations of Sn and O atoms within their sublattice and with respect to a sublattice of each other ($\sim$ 120 cm^{-1}), i.e. E$_{g(-1)}$

shown in Fig. 2. The other one is the out-of-plane vibration of two Sn atoms (~ 200 cm^{-1}), i.e. $E_{g(-2)}$ shown in Fig. 2. The secondary peak around 200 cm^{-1} of the monolayer (Fig. 3(a)) shows that the $E_{g(-2)}$ mode also has weak coupling with the electron in the strain-free condition. The major reason for the change in electron–phonon coupling is the effect of $\varepsilon = -1.0\%$ on the conduction band edge, especially around the M point. Additionally, the $E_{g(-1)}$ mode at the midpoint of the Γ–X line assists the intervalley electronic scattering between the valleys around the M point. Meanwhile, the phonon modes around the Γ point assist the intravalley electronic scattering.

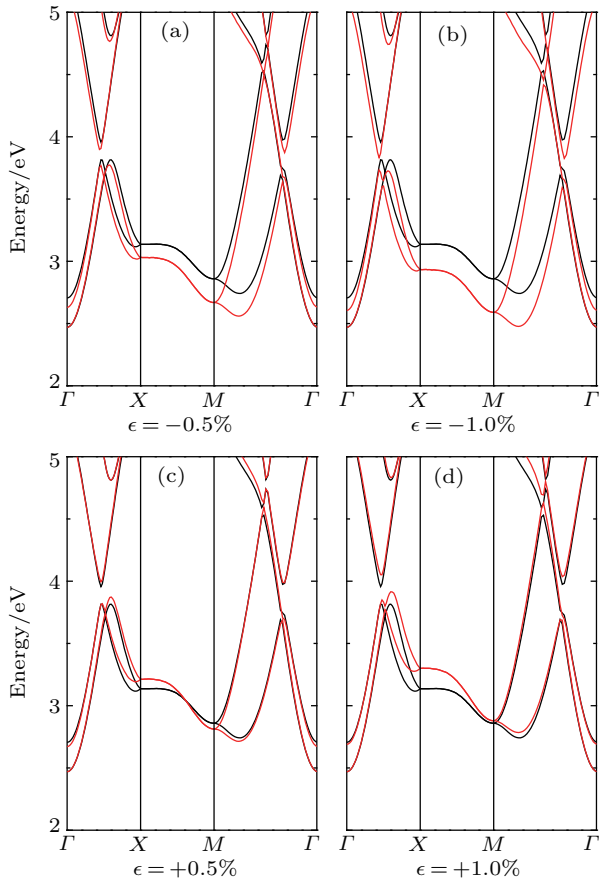


Fig. 4. Band structures under (a) and (b) compression strains ($\varepsilon = -0.5\%, -1.0\%$), and under (c) and (d) tensile strains ($\varepsilon = 0.5\%, 1.0\%$). The black line indicates the band structure of the strain-free monolayer SnO. The compression strains mainly influence the conduction band around the points X and M; tensile strains mainly influence the conduction band around the X point.

The transport spectral function α_{tr} under different strains also illustrates the significant change in electron–phonon coupling, as shown in Fig. 6(a). For the case of $\varepsilon = -1.0\%$, the main peak in the high-frequency region has a sharp decrease. The new peak around 120 cm^{-1} comes from the contribution of the $E_{g(-1)}$ mode coupling with electrons. According to Eq. (1), the small peak in the low-frequency region still produces large electron–phonon coupling. Therefore, the relaxation time τ of $\varepsilon = -1.0\%$ is lower than the prototypical monolayer. Finally, the strains considered in the present work have no remarkable influence on the electronic relaxation time, as shown in Fig. 6(b).

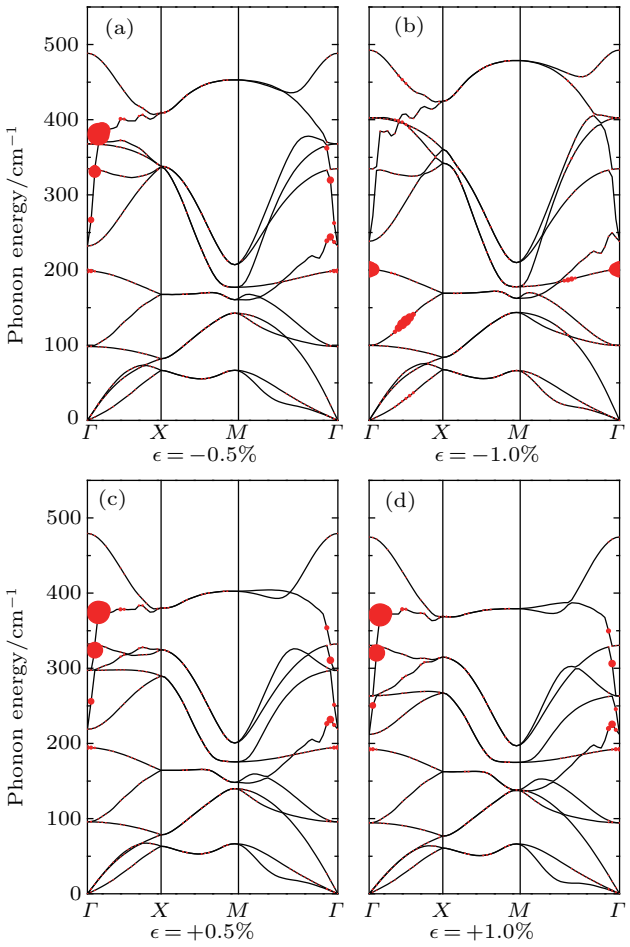


Fig. 5. Phonon spectra and phonon linewidths under (a) and (b) compression strains ($\varepsilon = -0.5\%, -1.0\%$), and under (c) and (d) tensile strains ($\varepsilon = 0.5\%, 1.0\%$). The large phonon linewidths mainly focus on the Γ point in the high-frequency region (350–400 cm^{-1}) except for $\varepsilon = -1.0\%$, which has large phonon linewidths at the Γ point and the midpoint of the $\Gamma - X$ line in the range of 150–200 cm^{-1}.

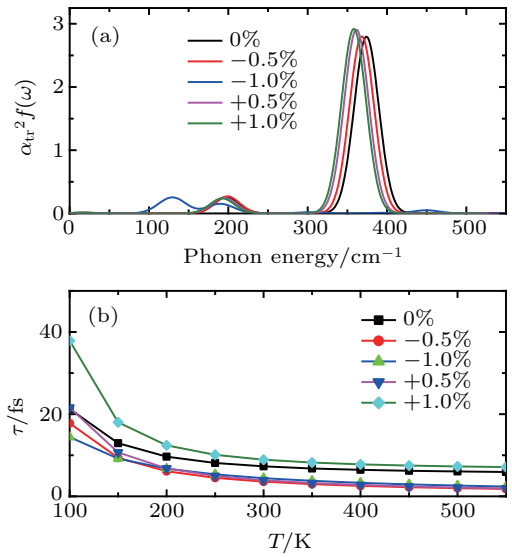


Fig. 6. (a) Transport spectral function α_{tr} and (b) the electronic relaxation time τ under compression strains ($\varepsilon = -0.5\%, -1.0\%$) and tensile strains ($\varepsilon = 0.5\%, 1.0\%$). The main peak appears at ~ 380 cm^{-1} in the high-frequency region except for $\varepsilon = -1.0\%$.

3.3. Mobility

The carrier mobility μ as a function of the temperature for the structures with different layers and various strains is plotted in Fig. 7. Firstly, μ of the bilayer is much higher than those of the monolayer and T-bilayer, due to the prominent change in conduction band edge as well as the electron–phonon coupling. At room temperature, the bilayer has $\mu = 76$ cm^2/(V·s) with six times the mobility of monolayer or T-bilayer, and the enhancement of the bilayer is more significant when the temperature drops (Fig. 7(a)), such as when 230 cm^2/(V·s) at 100 K. Secondly, the results show that there is no notable difference between carrier mobility under various strains (Fig. 7(b)). At room temperature, μ for all cases has a low value of ~ 10 cm^2/(V·s). The present results show that the N-type carrier mobility in the monolayer or bilayer SnO is much higher than the P-type carrier mobility obtained in the previous experiment.[19] Hence, the N-type ultrathin film of SnO may be more suitable for transistor devices.

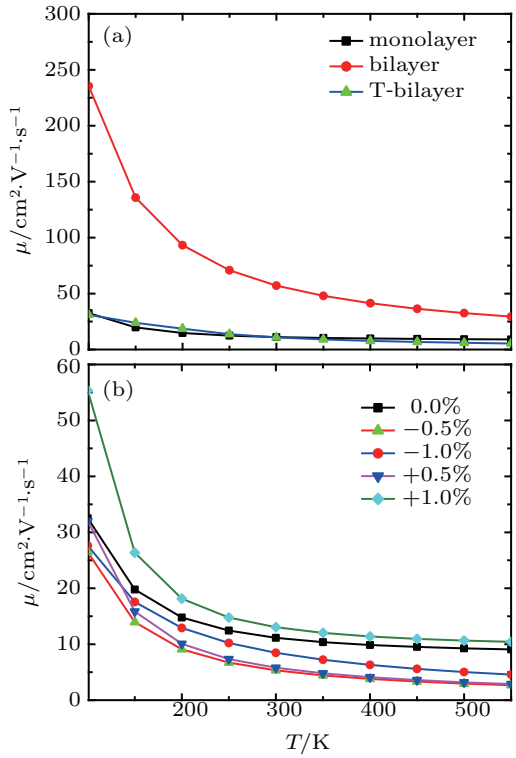


Fig. 7. Mobility μ as a function of the temperature T for the (a) monolayer, bilayer, and T-bilayer, and the (b) monolayer with various strains ($\varepsilon = -0.5\%$, -1.0%, 0.5%, and 1.0%).

4. Conclusion

In summary, we have studied the effect of the number of layers and strains on the phonon-limited mobility of SnO. In the strain-free condition, it is found that the coupling of the electron with the A_{2u} phonon mode in the high-frequency region is the strongest for the three types of layer structures. Furthermore, the interaction between Sn atoms from different layers in the bilayer structure obviously changes the CBM. Hence, the bilayer has the highest mobility of the three cases. After the introduction of strain in the monolayer structure, the compressive strain of $\varepsilon = -1.0\%$ leads to the CBM consisting of two valleys: one at the Γ point and one along the M–Γ line. Therefore, the intervalley electronic scattering assisted by the $E_{g(-1)}$ mode only appears in this case. However, the electron–phonon coupling regionally transferring from high frequency A_{2u} to low frequency $E_{g(-1)}$ results in little change in electronic transport; this is also present with other strains. This study provides fundamental information about the electron–phonon coupling and electronic transport property for in-depth research.

References

[1] Novoselov K S, Geim A K, Morozov S V, Jiang D, Zhang Y, Dubonos S V, Grigorieva I V and Firsov A A 2004 *Science* **306** 666
[2] Wang C, Liu X, Wang Z, Zhao M, He H and Zou J 2018 *Chin. Phys. B* **27** 118106
[3] Molle A, Goldberger J, Houssa M, Xu Y, Zhang S C and Akinwande D 2017 *Nat. Mater.* **16** 163
[4] Mannix A J, Kiraly B, Hersam M C and Guisinger N P 2017 *Nat. Rev. Chem.* **1** 0014
[5] Lew Yan Voon L C 2015 *Chin. Phys. B* **24** 87309
[6] Chhowalla M, Shin H S, Eda G, Li L J, Loh K P and Zhang H 2013 *Nat. Chem.* **5** 263
[7] Li S L, Tsukagoshi K, Orgiu E and Samori P 2016 *Chem. Soc. Rev.* **45** 118
[8] Zhou X, Gan L, Zhang Q, Xiong X, Li H, Zhong Z, Han J and Zhai T 2016 *J. Mater. Chem. C* **4** 2111
[9] Liu Y, Weiss N O, Duan X, Cheng H C, Huang Y and Duan X 2016 *Nat. Rev. Mater.* **1** 16042
[10] Anasori B, Lukatskaya M R and Gogotsi Y 2017 *Nat. Rev. Mater.* **2** 16098
[11] Mas-Balleste R, Gomez-Navarro C, Gomez-Herrero J and Zamora F 2011 *Nanoscale* **3** 20
[12] Gupta A, Sakthivel T and Seal S 2015 *Prog. Mater. Sci.* **73** 44
[13] Yang J and Y Lu Y 2017 *Chin. Phys. B* **26** 034201
[14] Wang F 2017 *Chin. Phys. B* **26** 034202
[15] Cocemasov A I, Isacova C I and Nika D L 2018 *Chin. Phys. B* **27** 56301
[16] Zhang Q, Zhang H and Cheng X L 2018 *Chin. Phys. B* **27** 27301
[17] Radisavljevic B, Radenovic A, Brivio J, Giacometti V and Kis A 2011 *Nat. Nanotechnol.* **6** 147
[18] Geim A K and Grigorieva I V 2013 *Nature* **499** 419
[19] Saji K J, Tian K, Snure M and Tiwari A 2016 *Adv. Electron. Mater.* **2** 1500453
[20] Xiao D, Liu G B, Feng W, Xu X and Yao W 2012 *Phys. Rev. Lett.* **108** 196802
[21] Zhou X, Zhang Q, Gan L, Li H, Xiong J and Zhai T 2016 *Adv. Sci.* **3** 1600177
[22] De D, Manongdo J, See S, Zhang V, Guloy A and Peng H 2013 *Nanotechnology* **24** 025202
[23] Song H S, Li S L, Gao L, Xu Y, Ueno K, Tang J, Cheng Y B and Tsukagoshi K 2013 *Nanoscale* **5** 9666
[24] Su G, Hadjiev V G, Loya P E, Zhang J, Lei S, Maharjan S, Dong P, Ajayan P M, Lou J and Peng H 2015 *Nano Lett.* **15** 506
[25] Huang Y, Sutter E, Sadowski J T, Cotlet M, Monti O L, Racke D A, Neupane M R, Wickramaratne D, Lake R K, Parkinson B A and Sutter P 2014 *ACS Nano* **8** 10743
[26] Su Y, Ebrish M A, Olson E J and Koester S J 2013 *Appl. Phys. Lett.* **103** 263104
[27] Zhou X, Gan L, Tian W, Zhang Q, Jin S, Li H, Bando Y, Golberg D and Zhai T 2015 *Adv. Mater.* **27** 8035
[28] Pan T S, De D, Manongdo J, Guloy A M, Hadjiev V G, Lin Y and Peng H B 2013 *Appl. Phys. Lett.* **103** 093108
[29] Kamal C, Chakrabarti A and Ezawa M 2016 *Phys. Rev. B* **93** 125428
[30] Chowdhury C, Karmakar S and Datta A 2017 *J. Phys. Chem. C* **121** 7615
[31] Sinsermsuksakul P, Chakraborty R, Kim S B, Heald S M, Buonassisi T and Gordon R G 2012 *Chem. Mater.* **24** 4556

[32] Xia J, Li X Z, Huang X, Mao N, Zhu D D, Wang L, Xu H and Meng X M 2016 *Nanoscale* **8** 2063
[33] Micoulaut M, Wenic W and Wuttig M 2008 *Phys. Rev. B* **78** 224209
[34] Wang R Y, Caldwell M A, Jeyasingh R G D, Aloni S, Shelby R M, Wong H S P and Milliron D J 2011 *J. Appl. Phys.* **109** 113506
[35] Chung K M, Wamwangi D, Woda M, Wuttig M and Bensch W 2008 *J. Appl. Phys.* **103** 083523
[36] Huang Y, Ling C, Liu H, Wang S and Geng B 2014 *J. Phys. Chem. C* **118** 9251
[37] Wang H and Qian X 2017 *2D Mater.* **4** 015042
[38] Wu M and Zeng X C 2016 *Nano Lett.* **16** 3236
[39] Fei R, Li W, Li J and Yang L 2015 *Appl. Phys. Lett.* **107** 173104
[40] Gomes L C, Carvalho A and Castro Neto A H 2015 *Phys. Rev. B* **92** 214103
[41] Hsieh T H, Lin H, Liu J, Duan W, Bansil A and Fu L 2012 *Nat. Commun.* **3** 982
[42] Yang G, Liu J, Fu L, Duan W and Liu C 2014 *Phys. Rev. B* **89** 085312
[43] Liu J, Qian X and Fu L 2015 *Nano Lett.* **15** 2657
[44] Seixas L, Rodin A S, Carvalho A and Castro Neto A H 2016 *Phys. Rev. Lett.* **116** 206803
[45] Watson G W 2001 *J. Chem. Phys.* **114** 758
[46] Izumi F 1981 *J. Solid State Chem.* **38** 381
[47] Moreno M S and Mercader R C 1994 *Phys. Rev. B* **50** 9875
[48] Zhou W and Umezawa N 2015 *Phys. Chem. Chem. Phys.* **17** 17816
[49] Hosono H, Ogo Y, Yanagi H and Kamiya T 2011 *Electrochem. Solid State Lett.* **14** 13
[50] Varley J B, Schleife A, Janotti A and Van de Walle C G 2013 *Appl. Phys. Lett.* **103** 082118
[51] Caraveo-Frescas J A, Nayak P K, Al-Jawhari H A, Granato D B, Schwingenschlogl U and Alshareef H N 2013 *ACS Nano* **7** 5160
[52] Lefebvre I, Szymanski M, Olivier-Fourcade J and Jumas J 1998 *Phys. Rev. B* **58** 1896
[53] Pannetier J and Denes G 1980 *Acta Crystallogr.* **36** 2763
[54] Pan X Q and Fu L 2001 *J. Electroceram.* **7** 35
[55] Togo A, Oba F, Tanaka I and Tatsumi K 2006 *Phys. Rev. B* **74** 195128
[56] Ogo Y, Hiramatsu H, Nomura K, Yanagi H, Kamiya T, Hirano M and Hosono H 2008 *Appl. Phys. Lett.* **93** 032113
[57] Liang L Y, Liu Z M, Cao H T, Yu Z, Shi Y Y, Chen A H, Zhang H Z, Fang Y Q and Sun X L 2010 *J. Electrochem. Soc.* **157** 598
[58] Quackenbush N F, Allen J P, Scanlon D O, Sallis S, Hewlett J A, Nandur A S, Chen B, Smith K E, Weiland C, Fischer D A, Woicik J C, White B E, Watson G W and Piper L F J 2013 *Chem. Mater.* **25** 3114
[59] Thomas G 1997 *Nature* **389** 907
[60] Ou C W, Dhananjay Ho Z Y, Chuang Y C, Cheng S S and Wu M C 2008 *Appl. Phys. Lett.* **92** 122113
[61] Lee H N, Kim H J and Kim C K 2010 *Jpn. J. Appl. Phys.* **49** 020202
[62] Nomura K, Kamiya T and Hosono H 2011 *Adv. Mater.* **23** 3431
[63] Qiang L, Liu W, Pei Y, Wang G and Yao R 2017 *Solid-State Electronics* **129** 163
[64] Wang H, Yu L L, Lee Y H, Shi Y M, Hsu A, Chin M L, Li L J, Dubey M, Kong J and Palacios T 2012 *Nano Lett.* **12** 4674
[65] Das S, Chen H Y, Penumatcha A V and Appenzeller J 2013 *Nano Lett.* **13** 100
[66] Li L, Yu Y, Ye G L, Ge Q, Ou X, Wu H, Feng D, Chen X H and Zhang Y 2014 *Nat. Nanotechnology* **9** 372
[67] He Y, Sobhani A, Lei S, Zhang Z, Gong Y, Jin Z, Zhou W, Yang Y, Zhang Y, Wang X, Yakobson B, Vajtai R, Halas N J, Li B, Xie E and Ajayan P 2016 *Adv. Mater.* **28** 5126
[68] Chen X D, Xin W, Jiang W S, Liu Z B, Chen Y and Tian J G 2016 *Adv. Mater.* **28** 2563
[69] Xin W, Chen X D, Liu Z B, Jiang W S, Gao X G, Jiang X Q, Chen Y and Tian J G 2016 *Adv. Optical Mater.* **4** 1703
[70] Cao Y, Fatemi V, Demir A, Fang S, Tomarken S L, Luo J Y, Sanchez-Yamagishi J D, Watanabe K, Taniguchi T, Kaxiras E, Ashoori R C and Jarillo-Herrero P 2018 *Nature* **556** 80
[71] Cao Y, Fatemi V, Fang S, Watanabe K, Taniguchi T, Kaxiras E and Jarillo-Herrero P 2018 *Nature* **556** 43
[72] Bissett M A, Tsujia M and Ago H 2014 *Phys. Chem. Chem. Phys.* **16** 11124
[73] Wu Y, Xia W, Gao W, Ren W and Zhang P 2017 *Phys. Rev. Appl.* **8** 034007
[74] Duerloo K A N, Li Y and Reed E J 2014 *Nat. Commun.* **5** 4214
[75] Rodin A S, Carvalho A and Castro Neto A H 2014 *Phys. Rev. Lett.* **112** 176801
[76] Zhu T and Ertekin E 2015 *Phys. Rev. B* **91** 205429
[77] Ge Y, Wan W, Feng W, Xiao D and Yao Y 2014 *Phys. Rev. B* **90** 035414
[78] Qiao J, Kong X, Hu Z X, Yang F and Ji W 2014 *Nat. Commun.* **5** 4475
[79] Allen P B 1978 *Phys. Rev. B* **17** 3725
[80] Gonze X 1997 *Phys. Rev. B* **55** 10337
[81] Gonze X and Lee C 1997 *Phys. Rev. B* **55** 10355
[82] Gonze X, Rignanese G M, Verstraete M, Beuken J M, Pouillon Y, Caracas R, Jollet F, Torrent M, Zerah G, Mikami M, Ghosez P, Veithen M, Raty J Y, Olevano V, Bruneval F, Reining L, Godby R, Onida G, Hamann D R and Allan D C 2005 *Z. Kristallogr.* **220** 558
[83] Gonze X, Amadon B, Anglade P M, *et al.* 2009 *Comput. Phys. Commun.* **180** 2582
[84] Hartwigsen C, Goedecker S and Hutter J 1998 *Phys. Rev. B* **58** 3641
[85] Baroni S, Gironcoli S D, Corso A D and Giannozzi P 2001 *Rev. Mod. Phys.* **73** 515